Hindawi Publishing Corporation
Advances in Materials Science and Engineering
Volume 2014, Article ID 606814, 10 pages
http://dx.doi.org/10.1155/2014/606814

Research Article

The Effects of Gallium Additions on Microstructures and Thermal and Mechanical Properties of Sn-9Zn Solder Alloys

Kang I. Chen,[1] Shou C. Cheng,[1] Chin H. Cheng,[2] Sean Wu,[1] Yeu-L. Jiang,[3] and Tsung-C. Cheng[4]

[1] *Department of Electronics Engineering and Computer Science, Tung Fang Design Institute, No. 110, Dong Fang Road, Hunei, Kaohsiung 82941, Taiwan*
[2] *Department of Aeronautics and Astronautics, Research Center for Energy Technology and Strategy, National Cheng Kung University, Tainan 70101, Taiwan*
[3] *Department of Electrical Engineering, National Chung Hsing University, Taichung 40227, Taiwan*
[4] *Department of Mechanical Engineering, National Kaohsiung University of Applied Sciences, Kaohsiung 80778, Taiwan*

Correspondence should be addressed to Kang I. Chen; kangichen@mail.tf.edu.tw

Received 19 September 2013; Revised 10 December 2013; Accepted 12 December 2013; Published 22 January 2014

Academic Editor: Tao Zhang

The effects of gallium additions on microstructures and thermal and mechanical properties of the Sn-9Zn solder alloys are investigated in this study. The results show that the melting temperature of the alloys decreases with the increase in the Ga concentration, while the pasty ranges of the alloys are simultaneously enlarged. By adding a 0.25–0.5 wt.% Ga element, the Sn-matrix region is slightly increased and the Zn-rich phase becomes slightly coarser; however, the overall microstructure is still very similar to that of the Sn-9Zn alloy. It is found that, when the Ga concentration is less than 0.50 wt.%, the ultimate tensile strength and elongation are maintained at the same values. The addition of a 0.25–0.50 wt.% Ga to the Sn-9Zn alloy also leads to small cup and cone fracture surfaces which exhibit near-complete ductile fracturing. With the addition being increased to 0.75 wt.%, larger cup and cone fractures are observed. The 1.00 wt.% Ga alloy has lower strength and ductility due to the coarser and nonuniform microstructures. However, the fracture surfaces of the 1.00 wt.% Ga alloy show partial cleavage and a partially dimpled fracture.

1. Introduction

Conventional Sn-Pb solders have commonly been used as the interconnection materials for soldering electronic components and devices. However, the use of Pb is restricted due to health and environmental issues. On the other hand, an alloy of Sn-Ag-Cu has been recognized as a potential lead-free solder even though Sn-Ag alloy systems have higher melting points (say, 216 to 221°C), as compared to an eutectic Sn-Pb alloy [1, 2]. A high melting point is accompanied by high soldering temperatures, which may give rise to substrate instability problems.

Recently, the Sn-9Zn alloy system has received increased interest since it features low cost, great mechanical properties, and a low eutectic temperature (198°C), close to that of the Sn-Pb alloy [2, 3]. The eutectic structure of the Sn-9Zn alloy system consists of two phases: a body centered tetragonal Sn matrix phase and a secondary phase of hexagonal Zn containing less than 0.039 at.% Sn in solid solution [3, 4]. However, the tendency of oxidation and poor wetting ability of this alloy system limits its application [5, 6]. In recent years, to overcome the shortfalls in the Sn-9Zn alloy, some authors have tried to add a third element, such as In [7], Ga [8], Bi [9–13], Al [14–18], Ag [19–22], Cr [23], Cu [24], and Ce/La [25–27], to the Sn-Zn binary system to improve the melting temperature, wettability, oxidation resistance, corrosion, and mechanical properties of the alloy. For example, McCormack and Jin [7] found that, as the element In is added to the Sn-Zn binary system, the wetting characteristics of the alloy can be improved and the melting temperature can be appreciably lowered. Kim et al. [9] reported that, with an addition of the element Bi, the melting point is decreased from 198.4

to 186.1°C. Lin and Liu [17, 18] added the Al element into the Sn-Zn alloy and showed that element Al can improve wetting properties and oxidation resistance. It has also been found that Sn-Zn-Ag solders [19] have good wettability on Cu substrates. Meanwhile, Wu et al. [25, 26] found that, by adding Ce/La into the Sn-Zn system, one could improve wettability, creep strength, and tensile strength.

The melting point of gallium is 29.78°C [29]. It has high thermal and electrical conductivity and reactivity with copper forming amalgams. In addition, its inherent characteristic of wetting most metals and oxides without the use of flux can be a very attractive property for microelectronic devices [30]. According to the Ga-Zn [31] and Ga- Sn [32], binary-phase diagrams, Ga may form solid solutions with Sn and Zn. There is a great need for a lead-free solder with the same melting point as the near-eutectic 63Sn-37Pb alloy.

Based on the existing information discussed above, most of the previous reports were focused on improving the melting temperature and wettability of the Sn-Zn alloy, and very few studies have been conducted to study the improvement in other thermal and mechanical properties. Therefore, the objective of this study is aimed at investigating the effects of adding gallium to the microstructures and the thermal and mechanical properties of a Sn-9Zn lead-free solder.

2. Materials and Experimental Methods

A series of alloys of tin, zinc, and gallium are prepared from pure elements (greater than 99.99% pure). The Ga content in the Sn-9Zn-xGa solders, represented by x, is varied between 0 and 1.0 wt.%. Table 1 shows the chemical composition of the solder alloys. The constituent elements have been melted in a quartz tube with an inside diameter of 8 mm under an argon atmosphere. The molten alloys (in the quartz tube) are homogenized at 800°C for 3 hours, the furnace cooled to 250°C, and then water (25°C) quenched, while the quartz tube jacket is still. The solder rods are then machined into tensile specimens with a 16 mm gauge length and 4 mm gauge diameter. Tensile tests are then performed at room temperature at a strain rate of 0.9 mm/min. The melting temperatures of the solder alloys are measured with differential scanning calorimetry (DSC). In the DSC analysis, a piece of solder about 10 mg is placed into an Al cell. For collecting the data of melting properties, the sample is initially scanned from 25°C to 300°C at a rate of 0.5°C/min under an argon atmosphere, then a phase identification of the various solders is carried out by using an X-ray diffractometer operated at 30 kV, and the Cu-Kα radiation is used at diffraction angles (2θ) from 35° to 47° with a scanning speed of 1°/min. The as-cast solders are sectioned, metallographically polished, and examined by using a scanning electron microscope (SEM). The composition of the precipitates and phases in the solidified solders are analyzed with an energy dispersive spectrometer (EDS) and a wavelength dispersive spectrometer (WDS).

Table 1: The chemical composition of the solder alloys.

The solder alloys	Zn (wt.%)	Ga (wt.%)	Sn (wt.%)
Sn-9Zn	9	0	Balance
Sn-9Zn-0.25Ga	9	0.25	Balance
Sn-9Zn-0.50Ga	9	0.50	Balance
Sn-9Zn-0.75Ga	9	0.75	Balance
Sn-9Zn-1.00Ga	9	1.00	Balance

3. Results and Discussion

3.1. The Thermal Properties of the Sn-Zn-xGa Alloys. Figure 1 shows the DSC curves of the Sn-Zn eutectic alloy and a series of Sn-9Zn-xGa alloys upon heating at a scanning rate of 0.5°C/min. The melting temperature of the alloys is decreased with an increase in the Ga concentration, but the pasty ranges of the alloys are simultaneously enlarged. A promising solder alloy should have a lower melting temperature and a narrow pasty temperature zone. As expected, the melting temperature for the Sn-9Zn-xGa alloy is decreased by increasing the Ga content. The melting temperature of Sn-9Zn, T_m, at its endothermic peak is 199.8°C. An addition of 0.5 wt.% Ga reduces the value of T_m to 198.8°C, and an addition of 1.0 wt.% Ga further reduces the value of T_m to 196.8°C. In the meantime, the addition of a small amount of Ga slightly expands the temperature interval of the pasty range, which is defined by the difference between the liquidus and solidus temperatures, $T_{\text{end}} - T_{\text{onset}}$, as shown in Figure 2. In this figure, it is observed that an addition of 0.25 wt.% Ga causes the measured pasty range of Sn-9Zn to change from 2.0 to 3.4°C, while an addition of an amount of 1.0 wt.% Ga increases the pasty range to 5.7°C, which is still lower than that of Sn-Pb eutectic [12], 11.5°C. A higher liquidus or melting temperature means a higher processing temperature is needed.

The comparison of solidus temperature (T_{onset}), liquidus temperature (T_{end}), pasty ranges ($T_{\text{end}} - T_{\text{onset}}$), melting temperature ($T_m$), A/m, and ΔH among various solder alloys measured by the DSC is provided in Table 2. Again, it is seen that an increase in the amount of Ga lowers the melting temperature of the solder. According to the Ga-Sn binary phase diagram, it is known that Ga may form solid solutions with Sn. The maximum solubility of Ga in Sn is 6.4 at.% at 20.7°C [32]. The eutectic temperature of Sn-Ga eutectic alloy is also 20.5°C, which could lower the melting point of the Sn-9Zn-xGa alloys. In addition, the eutectic temperature of the Zn-Ga eutectic alloy is 24.7°C, and the maximum solubility of Ga in Zn is about 3.87 at.% at 24.7°C [31]. Therefore, all melting temperatures of the Sn-9Zn-xGa solder alloys are lower than the eutectic temperatures of the Sn-9Zn eutectic alloy.

The heat of fusion (ΔH) can be determined by [33]

$$\Delta H = k\frac{A}{m}, \tag{1}$$

where k is a constant with a value of 2.64 for pure tin [33], m is the mass of the sample, and A is the area under the endothermic peak. From Table 2, A/m is determined as

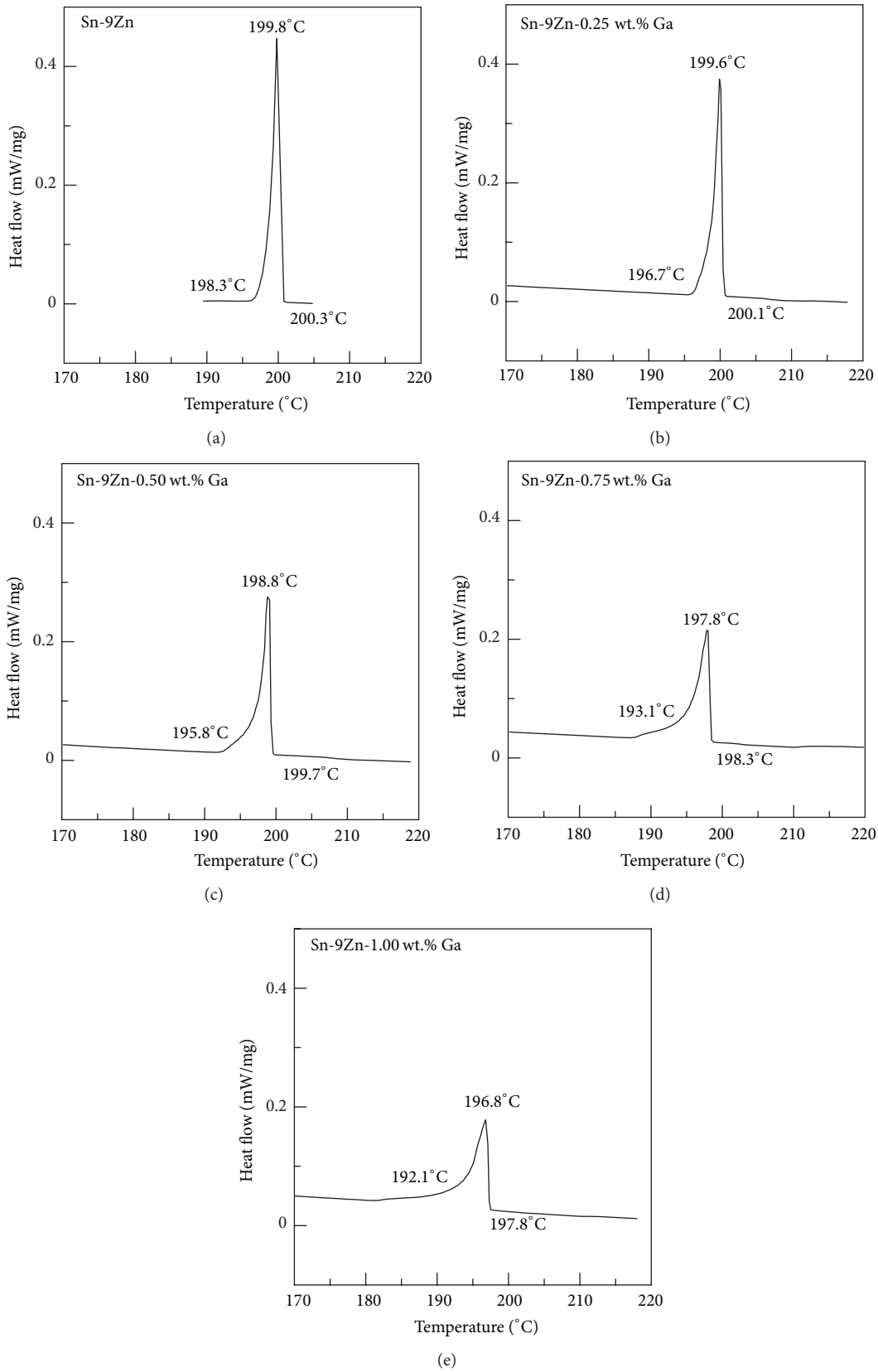

Figure 1: The DSC curves of the Sn-9Zn-xGa solder alloys containing (a) 0 wt.% Ga, (b) 0.25 wt.% Ga, (c) 0.50 wt.% Ga, (d) 0.75 wt.% Ga, and (e) 1.00 wt.% Ga upon heating at a scanning rate of 0.5°C/min.

Table 2: The comparison of solidus temperature (T_{onset}), liquidus temperature (T_{end}), pasty ranges (T_{end}-T_{onset}), melting temperature (T_m), A/m, and ΔH among various solder alloys.

Solder alloys	T_{onset} (°C)	T_{end} (°C)	T_{end} - T_{onset} (°C)	T_m (°C)	A/m (J/g)	ΔH (J/g)
Sn-9Zn	198.3	200.3	+2.0	199.8	70.2	185.3
Sn-9Zn-0.25Ga	196.7	200.1	+3.4	199.6	67.6	178.5
Sn-9Zn-0.50Ga	195.8	199.7	+3.9	198.8	62.4	164.7
Sn-9Zn-0.75Ga	193.1	198.3	+5.2	197.8	59.8	157.8
Sn-9Zn-1.00Ga	192.1	197.8	+5.7	196.8	57.2	151.0

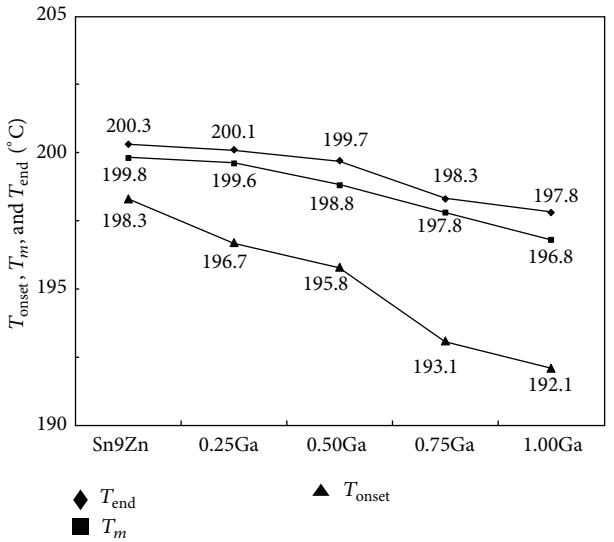

Figure 2: The solidus temperature (T_{onset}), melting temperature (T_m), and liquidus temperature (T_{end}) of various solder alloys.

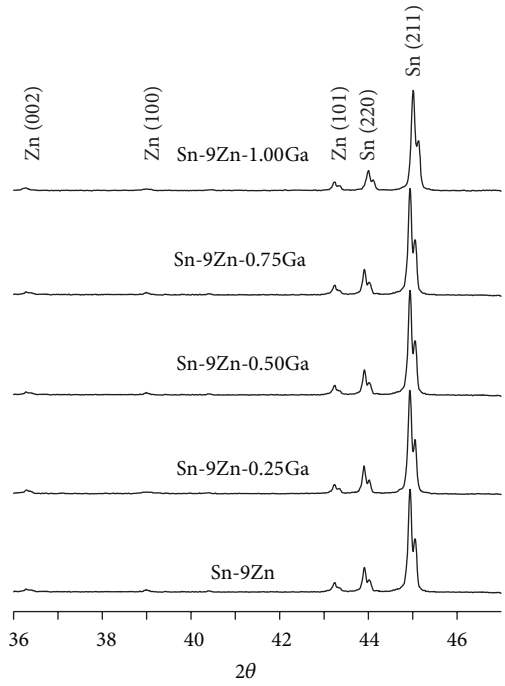

Figure 3: The XRD patterns of the Sn-9Zn, Sn-9Zn-0.25Ga, Sn-9Zn-0.50Ga, Sn-9Zn-0.75Ga, and Sn-9Zn-1.00Ga solder alloys.

70.2, 67.6, 62.4, 59.8, and 57.2 J/g for the Sn-9Zn, Sn-9Zn-0.25Ga, Sn-9Zn-0.5Ga, Sn-9Zn-0.75Ga, and Sn-9Zn-1.0Ga alloys, respectively. Consequently, the values of ΔH obtained are 185.3, 178.5, 164.7, 157.8, and 151.0 J/g for the Sn-9Zn, Sn-9Zn-0.25Ga, Sn-9Zn-0.5Ga, Sn-9Zn-0.75Ga, and Sn-9Zn-1.0Ga alloys, respectively, showing that it is necessary for energy to be consumed to melt the Sn-9Zn-xGa alloys.

3.2. X-Ray Diffractometry Analysis. The X-ray diffractometry (XRD) patterns of the Sn-9Zn, Sn-9Zn-0.25Ga, Sn-9Zn-0.5Ga, Sn-9Zn-0.75Ga, and Sn-9Zn-1.0Ga alloys are shown in Figure 3. The XRD analysis of the Sn-9Zn alloy displays the phases of the eutectic structure. The Bragg peaks corresponding to Sn(211), Sn(220), Zn(101), Zn(100), and Zn(002) are observed in the eutectic Sn-9Zn alloy. The Ga-Sn phase diagram [31] shows that Sn exhibits a maximum solubility of 6.4 at.% Ga. Meanwhile, the Ga-Zn phase diagram [31] shows that a hexagonal (Zn) solid solution possesses a maximum solubility of 2.36 at.% Ga at 260°C. The Ga-Sn and Ga-Zn binary phase diagrams indicate that Ga may form a solid solution with Sn and Zn. Thus, most of the Ga was dissolved in the Sn-rich and Zn-rich phases. The Sn-Zn exhibits a binary eutectic behavior with no intermetallic compounds and a limited solubility of the two elements in each phase. The results shown in this figure imply that the Sn-9Zn-0.25Ga, Sn-9Zn-0.5Ga, Sn-9Zn-0.75Ga, and Sn-9Zn-1.0Ga alloys only form Sn-matrixes and Zn-rich phases.

When the gallium content is increased, the XRD peaks of the Sn(211) phase shift toward the higher-angle regime, from 44.94° for Sn-9Zn to 45.01° for Sn-9Zn-1.0Ga, while the Zn(101) phase peak remains the same. Tin has the largest atomic radius (0.3022 nm); gallium has the smallest (0.2484 nm); and zinc has an atomic radius (0.2664 nm) between that of tin and gallium [29]. Therefore, when gallium atoms are dissolved in a Sn-rich phase, it seems reasonable that the lattice parameter of the Sn-rich phase is decreased.

3.3. Microstructures. The microstructures of the Sn-9Zn-xGa alloys are shown in Figure 4. The microstructure of the Sn-9Zn alloy is displayed in Figure 4(a). In this figure, the light contrasted areas indicate the Sn-rich phase (β-Sn), and the darker needle-like areas represent the Zn-rich phase. The cooling reaction at 250°C is L (liquid) → eutectic (Sn-Zn). As illustrated in Figures 4(b) and 4(c),

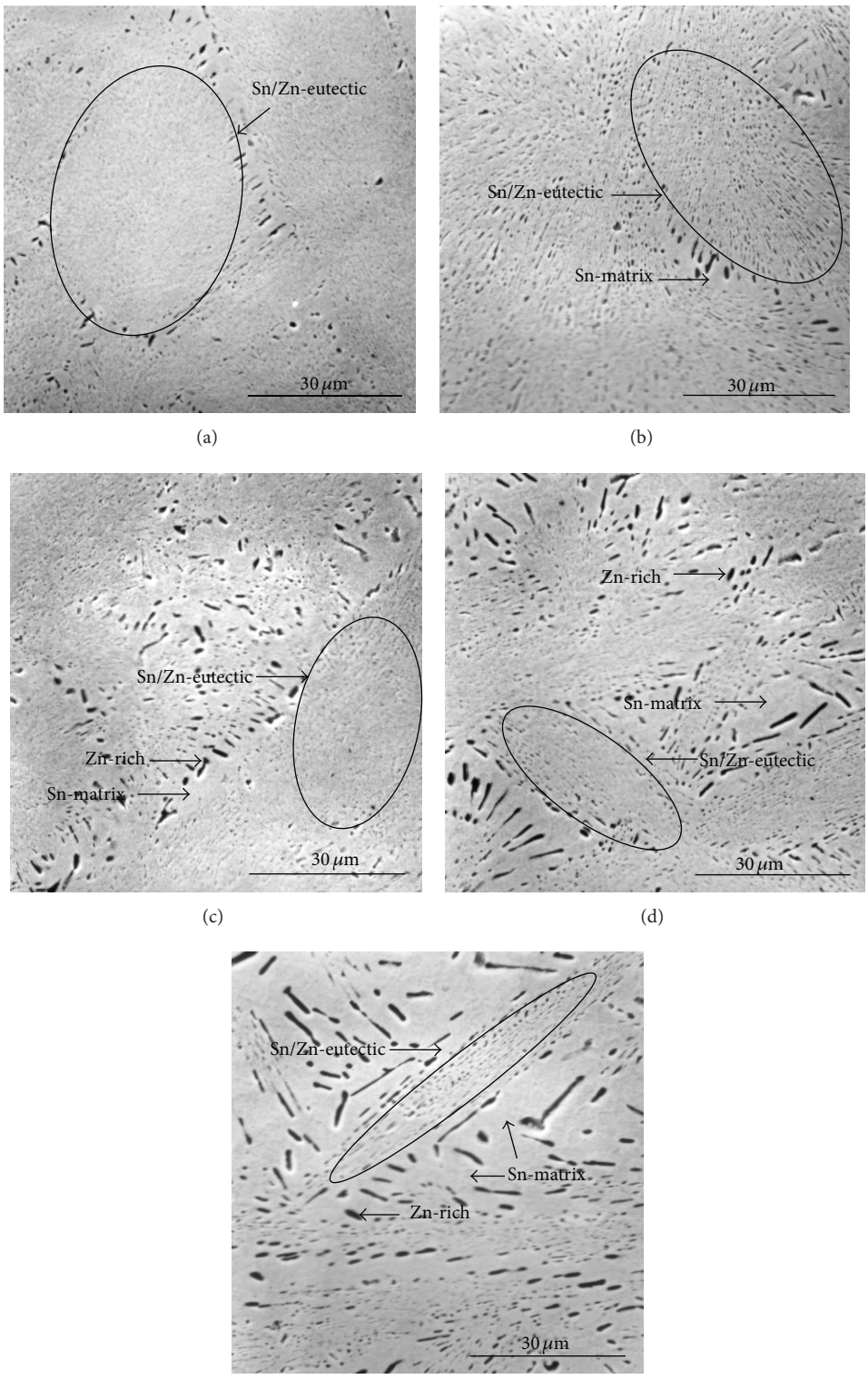

Figure 4: The SEM micrographs of the (a) Sn-9Zn, (b) Sn-9Zn-0.25Ga, (c) Sn-9Zn-0.50Ga, (d) Sn-9Zn-0.75Ga, and (e) Sn-9Zn-1.00Ga solder alloys.

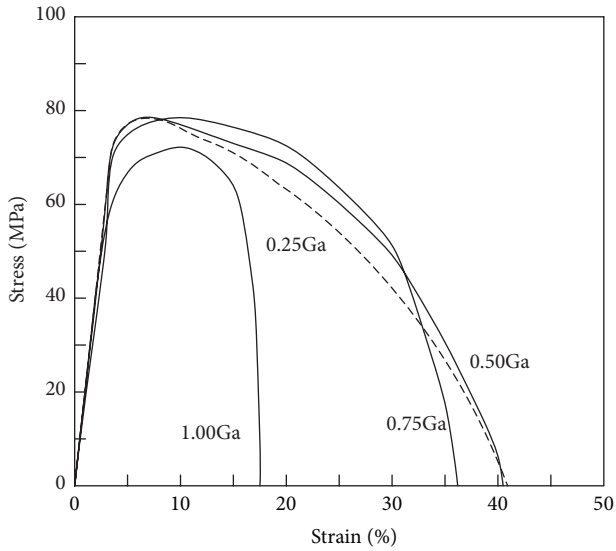

Figure 5: The tensile stress-strain curves of the Sn-9Zn, Sn-9Zn-0.25Ga, Sn-9Zn-0.50Ga, Sn-9Zn-0.75Ga, and Sn-9Zn-1.00Ga solder alloys.

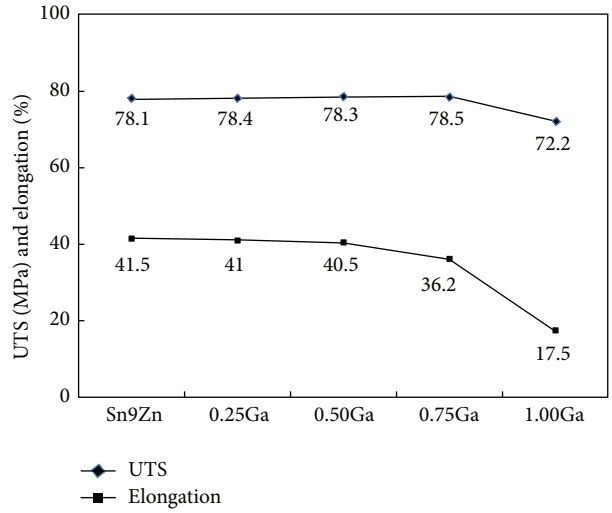

Figure 6: The tensile UTS and elongation of the Sn-9Zn-xGa alloys as a function of Ga concentration.

when 0.25–0.5 wt.% Ga is added, the Sn-matrix areas slightly increase and the Zn-rich areas become slightly coarser, but the overall microstructures are very similar to those of the Sn-9Zn alloy. The solder containing 1.00 wt.% Ga exhibits coarser nonuniform microstructures which contain large and long needle-like Zn-rich precipitates. The cooling reaction at 250°C is L (liquid) $\rightarrow$ primary Sn + eutectic (Sn-Zn). This result is consistent with the XRD results. The phase diagram of Sn-Zn shows a typical eutectic phase diagram with no intermetallic compounds and a limited solubility of the two elements in each phase.

Due to the addition of the Ga element, the Zn-rich phase precipitates grow and disperse in the β-Sn matrix, which can be observed in Figures 4(d) and 4(e). In addition, by increasing the content of the Ga element, the fraction of the Sn/Zn eutectic region decreases, the Sn-matrix region increases, and the needle-like Zn-rich phase becomes coarser and longer.

3.4. Mechanical Properties. The effect of the addition of Ga to the mechanical properties can be seen from the stress-strain curves shown in Figure 5. The ultimate tensile strength (UTS) of the Sn-9Zn, Sn-9Zn-0.25Ga, Sn-9Zn-0.50Ga, Sn-9Zn-0.75Ga, and Sn-9Zn-1.00Ga solder alloys is 78.1 MPa, 78.4 MPa, 78.3 MPa, 78.5 MPa, and 72.2 MPa, respectively. The elongation failure of the Sn-9Zn, Sn-9Zn-0.25Ga, Sn-9Zn-0.50Ga, Sn-9Zn-0.75Ga, and Sn-9Zn-1.00Ga solder alloys is 41.5%, 41.0%, 40.5%, 36.2%, and 17.5%, respectively. That is, with the addition of 0.25–0.50 wt.% Ga to Sn-9Zn alloy, the UTS and elongation appear not to have been changed. The Sn-9Zn, Sn-9Zn-0.25Ga, and Sn-9Zn-0.5Ga alloys exhibit proper UTS and elongation behavior because of uniform microstructures. However, when the addition is increased to 1.00 wt.%, the alloy displays an appreciable change in mechanical properties. The strength and ductility of the 1.00 wt.% Ga alloy are greatly reduced. This is probably due to the coarser nonuniform microstructures with larger and longer needle-like Zn-rich precipitates in the alloy. The 1.0 wt.% Ga addition to the Sn-9Zn alloy shown in Figure 4(e) destroys the uniform eutectic structure and needle-like precipitate of the Zn-rich phase, and the hypoeutectic β-Sn matrix. This alloy exhibits a more coarser nonuniform microstructure. The β-Sn matrix and the Zn-rich phase are coarser than those of the Sn-9Zn alloy. The Sn-Zn eutectic regions, with fine dispersion of Zn-rich precipitates, are stronger than the β-Sn matrix. This type of microstructure may profoundly degrade the mechanical properties of the alloy. The degradation in the mechanical property is due to the nonuniform distribution of the hard Sn-Zn eutectic regions, leading to a preferred crack growth at the softer β-Sn matrix regions.

The tensile strength, elongation, and fracture pattern of the Sn-37Pb [28] and Sn-9Zn-xGa solder alloys are summarized in Table 3. The Sn-9Zn-(0~0.75)Ga alloys had higher UTS and elongation, while the Sn-37Pb and Sn-9Zn-1.0Ga had lower UTS and elongation.

The tensile stress and strain of the Sn-9Zn-xGa alloys are shown as functions of the Ga concentration in Figure 6. It is clearly seen that if the Ga concentration is not beyond 0.50 wt.%, the ultimate tensile strength and elongation are fixed at the same values of 78 MPa and 41%, respectively. With the addition of 1.0 wt.% Ga, the UTS and elongation of the alloy are decreased to approximately 72.2 MPa and 17.5%, respectively, which means that there is an 8% and a 57% drop in the UTS and elongation, respectively, as compared to the 0.25 wt.% Ga alloy.

The addition of 1.0 Ga into the Sn-9Zn alloy diminishes the eutectic structure and β-Sn matrix (Figure 4(e)). It is accompanied by a coarsening of microstructure matrix. Thus, the UTS drops from 78.1 MPa in the Sn-9Zn to 72.2 MPa in the Sn-9Zn-1.00Ga alloy. The large decrease in UTS

Table 3: The mechanical properties of the Sn-37Pb and Sn-9Zn-xGa solder alloys.

Solder alloys	Tensile strength (MPa)	Elongation (%)	Fracture pattern	Reference
Sn-37Pb	55.0	37.5	Dimple	[28]
Sn-9Zn	78.1	41.5	Dimple	This study
Sn-9Zn-0.25Ga	78.4	41.0	Dimple	This study
Sn-9Zn-0.50Ga	78.3	40.5	Dimple	This study
Sn-9Zn-0.75Ga	78.5	36.2	Dimple	This study
Sn-9Zn-1.00Ga	72.2	17.5	Cleavage + dimple	This study

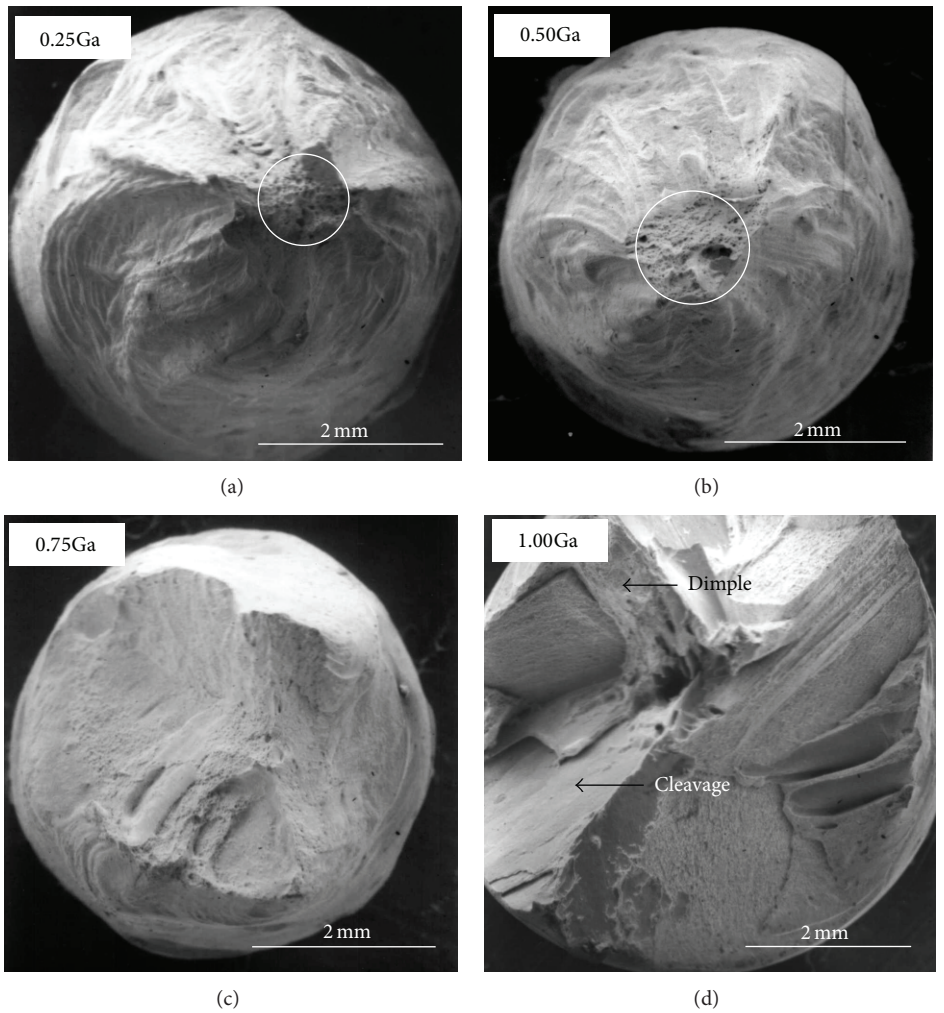

Figure 7: The fracture surfaces of the Sn-9Zn-0.25Ga, Sn-9Zn-0.50Ga, Sn-9Zn-0.75Ga, and Sn-9Zn-1.00Ga solder alloys.

caused by 1.0 Ga additions to the Sn-9Zn alloy is due to a fraction of the Sn/Zn eutectic region decreasing, the Sn-matrix region increasing, and the needle-like Zn-rich phase becoming coarser and longer. The Ga-Zn phase diagram [31] shows that hexagonal (Zn) solid solution possesses a maximum solubility of 2.36 at.% Ga at 260°C. Meanwhile, Sn exhibits [32] a maximum solubility of 7.1 at.% Ga. Thus, most of the Ga is dissolved in the Sn-rich and Zn-rich phases. The atomic radii of tin, zinc, and gallium have nearly the same size. Thus, when Ga is added to the Sn-9Zn alloy, it may form a solid solution structure. It is believed that strengthening effect of the Ga addition is attributed to the dissolution of Ga in Sn. However, the strengthening effect of the Ga is not improved by increasing Ga content, as the Ga element has a small atom size. This contributes to the formation of the needle-like precipitate of the Zn-rich phases and the hypoeutectic β-Sn matrix, while the eutectic cell boundary becomes prominent in the matrix. The tensile strain is obviously decreased because stress concentration occurs at the interface between either the hard Zn-rich phases or the Sn-Zn eutectic regions and the β-Sn matrix.

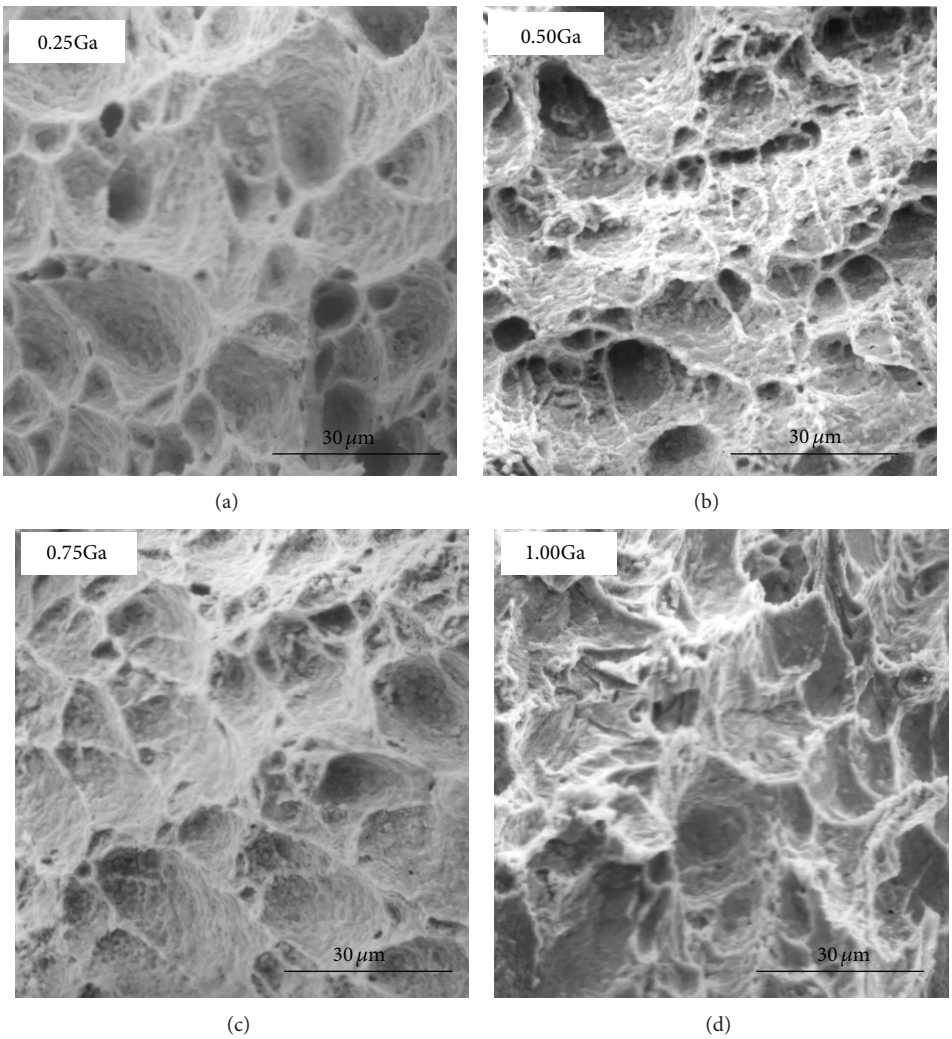

Figure 8: A higher magnification of the fracture surfaces of Sn-9Zn-0.25Ga, Sn-9Zn-0.50Ga, Sn-9Zn-0.75Ga and Sn-9Zn-1.00Ga solder alloys.

3.5. Fracture Morphology. Figure 7 shows the scanning electron microscopy (SEM) of the fracture surfaces of four of the tensile specimens made from Sn-9Zn-0.25Ga, Sn-9Zn-0.50Ga, Sn-9Zn-0.75Ga, and Sn-9Zn-1.00Ga solder alloys. A higher magnification of the fracture surfaces of the four alloys is provided in Figure 8. It was found that an additional 0.25–0.50 wt.% small-sized cup and cone fracture, which is referred to as a near-complete ductile fracture, is observed within. With the addition of a 0.75 wt.%, the size of the cup and cone fracture becomes larger. The fracture surface of the 1.00 wt.% Ga alloy displays partial cleavage and a partially dimpled fracture, which are indicated by the circles in Figure 7. This indicates a reduction in the ductility of the alloy taking place at 1.00 wt.% Ga, which is due to the formation of larger and longer needle Zn-rich precipitates and of the coarser and nonuniform microstructures. According to the work of Kim et al. [9], the fractures of the Sn-8Zn-6Bi and Sn-8Zn-8Bi alloys show a typical brittle-fracture pattern and fractures occur along the coarse dendrite or long Zn precipitates.

4. Conclusions

The present study is concerned with the effects of a gallium addition on microstructures and thermal and mechanical properties of Sn-9Zn solder alloys. The results show that the melting temperatures of the alloys decrease with an increase in Ga concentration, while the pasty ranges of the alloys are simultaneously enlarged. The experimental results also show that the addition of the Ga element causes the Zn-rich phase precipitates to grow and disperse in the β-Sn matrix. In addition, by increasing the content of the Ga element, the fraction of the Sn/Zn eutectic region decreases, the Sn-matrix region increases, and the needle-like Zn-rich phase becomes coarser and longer. However, the overall microstructure is still very similar to that of the Sn-9Zn alloy. Meanwhile, small additions of 0~0.75 wt.% Ga decrease the melting point of the Sn-9Zn-xGa solders while maintaining the same strength and ductility as the Sn-9Zn solder; one also observes small cup and cone fractures on the fracture surfaces which exhibit near-complete ductile fractures. As the addition is increased

to 0.75 wt.%, larger cup and cone fractures are seen. The 1.00 wt.% Ga alloy has a lower strength and ductility due to the coarser and nonuniform microstructures. However, the fracture surfaces of the 1.00 wt.% Ga alloy show only a partially cleaved and partially dimpled fracture.

Conflict of Interests

The authors declare that there is no conflict of interests regarding the publication of this paper.

Acknowledgment

The authors acknowledge the financial support provided by the National Science Council of the Republic of China.

References

[1] M. McCormack and S. Jin, "Progress in the design of new lead-free solder alloys," *The Journal of the Minerals, Metals & Materials Society*, vol. 45, no. 7, pp. 36–40, 1993.

[2] M. Abtew and G. Selvaduray, "Lead-free solders in microelectronics," *Materials Science and Engineering R*, vol. 27, no. 5, pp. 95–141, 2000.

[3] H. Mavoori, J. Chin, S. Vaynman, B. Moran, L. Keer, and M. Fine, "Creep, stress relaxation, and plastic deformation in Sn-Ag and Sn-Zn eutectic solders," *Journal of Electronic Materials*, vol. 26, no. 7, pp. 783–790, 1997.

[4] K. Suganuma, T. Murata, H. Noguchi, and Y. Toyoda, "Heat resistance of Sn-9Zn solder/Cu interface with or without coating," *Journal of Materials Research*, vol. 15, no. 4, pp. 884–891, 2000.

[5] E. P. Wood and K. L. Nimmo, "In search of new lead-free electronic solders," *Journal of Electronic Materials*, vol. 23, no. 8, pp. 709–713, 1994.

[6] K. Suganuma, K. Niihara, T. Shoutoku, and Y. Nakamura, "Wetting and interface microstructure between Sn-Zn binary alloys and Cu," *Journal of Materials Research*, vol. 13, no. 10, pp. 2859–2865, 1998.

[7] M. McCormack and S. Jin, "New, lead-free solders," *Journal of Electronic Materials*, vol. 23, no. 7, pp. 635–640, 1994.

[8] K. Chen, S. Cheng, S. Wu, and K. Lin, "Effects of small additions of Ag, Al, and Ga on the structure and properties of the Sn-9Zn eutectic alloy," *Journal of Alloys and Compounds*, vol. 416, no. 1-2, pp. 98–105, 2006.

[9] Y. Kim, K. Kim, C. Hwang, and K. Suganuma, "Effect of composition and cooling rate on microstructure and tensile properties of Sn-Zn-Bi alloys," *Journal of Alloys and Compounds*, vol. 352, no. 1-2, pp. 237–245, 2003.

[10] M. Date, K. N. Tu, T. Shoji, M. Fujiyoshi, and K. Sato, "Interfacial reactions and impact reliability of Sn-Zn solder joints on Cu or electroless Au/Ni(P) bond-pads," *Journal of Materials Research*, vol. 19, no. 10, pp. 2887–2896, 2004.

[11] A. Hirose, H. Yanagawa, E. Ide, and K. F. Kobayashi, "Joint strength and interfacial microstructure between Sn-Ag-Cu and Sn-Zn-Bi solders and Cu substrate," *Science and Technology of Advanced Materials*, vol. 5, no. 1-2, pp. 267–276, 2004.

[12] A. A. El-Daly, Y. Swilem, M. H. Makled, M. G. El-Shaarawy, and A. M. Abdraboh, "Thermal and mechanical properties of Sn-Zn-Bi lead-free solder alloys," *Journal of Alloys and Compounds*, vol. 484, no. 1-2, pp. 134–142, 2009.

[13] S. Wang, T. Chin, C. Yang, S. Chen, and C. Chuang, "Pb-free solder-alloy based on Sn-Zn-Bi with the addition of germanium," *Journal of Alloys and Compounds*, vol. 497, no. 1-2, pp. 428–431, 2010.

[14] K. Lin, L. Wen, and T. Liu, "The microstructures of the Sn-Zn-Al solder alloys," *Journal of Electronic Materials*, vol. 27, no. 3, pp. 97–105, 1998.

[15] K. Lin and Y. Wang, "Wetting interaction of Pb-free Sn-Zn-Al solders on metal plated substrate," *Journal of Electronic Materials*, vol. 27, no. 11, pp. 1205–1210, 1998.

[16] K. Lin and L. Wen, "The wetting of copper by Al-Zn-Sn solders," *Journal of Materials Science*, vol. 9, no. 1, pp. 5–8, 1998.

[17] K. Lin and T. Liu, "High-temperature oxidation of a Sn-Zn-Al solder," *Oxidation of Metals*, vol. 50, no. 3-4, pp. 255–267, 1998.

[18] K. Lin and T. Liu, "The electrochemical corrosion behaviour of Pb-free Al-Zn-Sn solders in NaCl solution," *Materials Chemistry and Physics*, vol. 56, no. 2, pp. 171–176, 1998.

[19] K. Lin and C. Shih, "Wetting interaction between Sn-Zn-Ag solders and Cu," *Journal of Electronic Materials*, vol. 32, no. 2, pp. 95–100, 2003.

[20] J. M. Song, G. F. Lan, T. S. Lui, and L. H. Chen, "Microstructure and tensile properties of Sn-9Zn-*x*Ag lead-free solder alloys," *Scripta Materialia*, vol. 48, no. 8, pp. 1047–1051, 2003.

[21] J. M. Song, T. S. Lui, G. F. Lan, and L. H. Chen, "Resonant vibration behavior of Sn-Zn-Ag solder alloys," *Journal of Alloys and Compounds*, vol. 379, no. 1-2, pp. 233–239, 2004.

[22] G. Saad, A. Fawzy, and E. Shawky, "Effect of Ag addition on the creep characteristics of Sn-8.8 wt%Zn solder alloy," *Journal of Alloys and Compounds*, vol. 479, no. 1-2, pp. 844–850, 2009.

[23] X. Chen, A. Hu, M. Li, and D. Mao, "Study on the properties of Sn-9Zn-*x*Cr lead-free solder," *Journal of Alloys and Compounds*, vol. 460, no. 1-2, pp. 478–484, 2008.

[24] J. Lee, K. Kim, M. Inoue, J. Jiang, and K. Suganuma, "Effects of Ag and Cu addition on microstructural properties and oxidation resistance of Sn-Zn eutectic alloy," *Journal of Alloys and Compounds*, vol. 454, no. 1-2, pp. 310–320, 2008.

[25] C. M. L. Wu, D. Q. Yu, C. M. T. Law, and L. Wang, "The properties of Sn-9Zn lead-free solder alloys doped with trace rare earth elements," *Journal of Electronic Materials*, vol. 31, no. 9, pp. 921–927, 2002.

[26] C. M. L. Wu, C. M. T. Law, D. Q. Yu, and L. Wang, "The wettability and microstructure of Sn-Zn-RE alloys," *Journal of Electronic Materials*, vol. 32, no. 2, pp. 63–69, 2003.

[27] C. M. L. Wu, D. Q. Yu, C. M. T. Law, and L. Wang, "Properties of lead-free solder alloys with rare earth element additions," *Materials Science and Engineering R*, vol. 44, no. 1, pp. 1–44, 2004.

[28] K. Chen and K. Lin, "The microstructures and mechanical properties of the Sn-Zn-Ag-Al-Ga solder alloys—the effect of Ag," *Journal of Electronic Materials*, vol. 31, no. 8, pp. 861–867, 2002.

[29] M. Hansen, *Constitution of Binary Alloys*, McGraw-Hill Book, New York, NY, USA, 2nd edition, 1958.

[30] S. K. Bhattacharya and D. F. Baldwin, "Gallium alloy breakthrough for via-filling application," *Advanced Packaging*, vol. 9, no. 8, pp. 61–64, 2000.

[31] J. Dutkiewicz, Z. Moser, L. Zabdyr et al., "The Ga-Zn (gallium-zinc) system," *Bulletin of Alloy Phase Diagrams*, vol. 11, no. 1, pp. 77–82, 1990.

[32] T. J. Anderson and I. Ansara, "The Ga-Sn (gallium-tin) system," *Journal of Phase Equilibria*, vol. 13, no. 2, pp. 181–189, 1992.

[33] A. A. El-Daly, Y. Swilem, and A. E. Hammad, "Creep properties of Sn-Sb based lead-free solder alloys," *Journal of Alloys and Compounds*, vol. 471, no. 1-2, pp. 98–104, 2009.